Crystal Structure and Compressibility of $Ba_4Ru_3O_{10}$

A. H. Carim,*,†,[1] P. Dera,†,‡ L. W. Finger,† B. Mysen,† C. T. Prewitt,† and D. G. Schlom*

*Department of Materials Science and Engineering, The Pennsylvania State University, University Park, Pennsylvania 16802-5005;
†Geophysical Laboratory, Carnegie Institution of Washington, Washington, D.C., 20015-1305; and
‡Department of Crystal Chemistry, Adam Mickiewicz University, 60–780 Poznan, Poland

The crystal structure of $Ba_4Ru_3O_{10}$ has been determined by single-crystal X-ray diffraction at room pressure. From refinements to $R = 0.0203$ at room temperature and ambient pressure, the material is orthorhombic with space group *Cmca* (space group No. 64) and has lattice parameters of $a = 5.7762(15)$ Å, $b = 13.271(4)$ Å, and $c = 13.083(3)$ Å. The unit cell thus has a volume of $V = 1002.9(8)$ Å^3 and contains four formula units ($Z = 4$). $Ba_4Ru_3O_{10}$ is therefore of higher symmetry than the previously reported monoclinic structure based on powder X-ray data. It is isostructural with the quaternary oxides $Ba_4(Ti, Pt)_3O_{10}$ and $Ba_4Ir_2AlO_{10}$ and the ternary fluorides $Cs_4M_3F_{10}$ ($M = $ Mg, Co, Ni, Zn). Kinked chains of RuO_6 octahedra run along the *c* direction, consisting of sets of three face-sharing units joined at the corners of the end units to additional similar sets. The two distinct Ba sites show 10-fold and 11-fold coordination. Compressibilities and bulk modulus have been determined from lattice parameter variations at pressures up to 5.4 GPa. No phase transition was observed up to this pressure. Compressibility is greatest along the *c* axis and the bulk modulus obtained from a weighted fit to a Vinet equation of state is 113.3(47) GPa. © 2000 Academic Press

Key Words: ruthenates; crystal structure; compressibility; bulk modulus; high pressure.

INTRODUCTION

Although numerous barium ruthenates have been reported ($BaRuO_3$ (1–4), $BaRu_4O_9$ (4), $BaRu_6O_{12}$ (5), Ba_2RuO_4 (3, 4, 6, 7), Ba_3RuO_5 (3, 4), $Ba_4Ru_3O_{10}$ (8), $Ba_5Ru_3O_{12}$ (8), Ba_4RuO_6 (3), and Ba_9RuO_{11} (3)), crystal structures have not been established for all of these compounds, and relatively few (specifically $BaRuO_3$, $BaRu_6O_{12}$, and $Ba_5Ru_3O_{12}$) have been synthesized and analyzed in single-crystal form. The phases with $Ba_{n+1}Ru_nO_{3n+1}$ stoichiometries are particularly interesting because of the possibility that they may form in layered

perovskite (Ruddlesden–Popper) structures (9–11), although this appears to require high pressures (7). In this report we describe single-crystal X-ray diffraction of $Ba_4Ru_3O_{10}$ at pressures up to 5.4 GPa. The crystal structure is found to be similar to, but of higher symmetry than, the monoclinic structure derived earlier from powder diffraction (8). No phase transitions to the layered perovskite or other forms are observed within this pressure range.

EXPERIMENTAL PROCEDURE

Sample Synthesis

The phase described here was obtained as crystals within multiphase samples, in the course of investigating ternary compounds in the Ba–Ru–O system. Initial powders of $BaCO_3$ (Alfa Aesar, 99.997% metals basis) and RuO_2 (Alfa Aesar, 99.95% metals basis) were combined so as to provide a Ba : Ru ratio of 2 : 1. The mixture was ground (dry) in an agate mortar for 45–60 min and then pressed into a pellet at $\sim$180 MPa and 120°C for 10–15 min. Pellets were then suspended in a platinum wire cage and annealed for 95 h at 1400°C and a $f(O_2) = 10^{-3}$ (for the single crystal analyzed) or at 1300°C and a $f(O_2) = 10^{-4}$ (giving similar results); oxygen fugacity was controlled by mixing flowing CO and CO_2 gases and monitored with an yttria-stabilized ZrO_2 sensor. The low oxygen fugacity was used to try to cause the reaction to proceed without loss of ruthenium via oxidation to volatile higher oxides such as RuO_4; in the absence of sufficient data for Ba–Ru–O systems, the $f(O_2)$ values used were selected on the basis of extrapolations from earlier work in the Sr–Ru–O system (12).

The compositions of the barium ruthenate grains in polished sample sections were analyzed by quantitative wavelength-dispersive spectroscopy in an electron microprobe. The crystals were homogeneous and found to have a nearly stoichiometric composition of $Ba_{4.04(2)}Ru_{2.98(1)}O_{10}$ (averages and standard deviations from 7 grains, assuming 10 oxygen atoms per formula unit). The crystal used and those analyzed by a microprobe were chosen from

---

TABLE 1
Crystallographic Data, Collection Conditions, and Refinement Parameters for Ba₄Ru₃O₁₀

Crystallographic Data	
Symmetry	Orthorhombic (*Cmca*, No. 64)
Cell parameters (Å)	$a = 5.7762(15)$, $b = 13.271(4)$, $c = 13.083(3)$
Volume (Å³)	1002.9(8)
Z	4
Calculated density (g cm⁻³)	6.71
Data Collection ($T = 20°C$)	
Crystal shape and size	Parallelepiped, approx. $20 \times 50 \times 60$ μm³
Diffractometer	Bruker AXS P4 four-circle
Detector	SMART 1000 CCD (1K)
Source of radiation	X-ray tube w/graphite monochromator (Mo$K\alpha$)
No. of frames acquired	1650 (in 5 scans)
Scan step size (°)	0.3
Average peak half-width (°)	0.5
Minimum d_{hkl} (Å)	0.72
No. of measured reflections	2251
No. of reflections used for refinement	684
No. of independent reflections	684
Transmission coefficient range	0.376–0.550
Structural Refinement	
Programs used	SAINT (Bruker's, Data processing) XPREP (Bruker's, absorption correction) SHELXS (structure solution) SHELXL (anisotropic refinement)
Extinction parameter	0.001689
No. of refined parameters	50
Merging R factor R_{int}	0.0764
Reliability factor R_1	0.0203 (595 data with $F_0 > 4\sigma(F_0)$) 0.0276 (all data)
Reliability factor wR_2	0.0638 (all data)

sections away from the contact points of the Pt wire cage with the sample, and thus it is believed that little or no Pt is incorporated therein; Pt was not detected in energy-dispersive spectroscopy (EDS) or WDS scans of any grains.

Ambient-Pressure Measurements and Structure Determination

Data on the crystal selected for structure determination, the unit cell parameters measured at ambient pressure, and the experimental parameters are given in Table 1. The structural determination was carried out with an automated Bruker AXS P4 system equipped with a SMART 1000 CCD area detector. The instrument employs Mo$K\alpha$ radiation and the generator was set at 50 kV and 40 mA. A hemisphere of data to 0.72 Å was collected with 0.3° frames, with 88.1% coverage of this reciprocal space region and a mean $I/\sigma = 13.32$. Counting time for each frame was 10 s. The data were corrected for geometrical distortion, dark current,

and flood-field effects. Integrated intensities were extracted using Bruker software and the data were corrected for Lorentz and polarization effects. Data merging, both for redundant reflections and the symmetrical equivalents, and an absorption correction using an ellipsoid model were performed with the program XPREP from the SHELXTL package supplied by Bruker AXS. Occupancies of the atomic sites have not been refined. A stoichiometric composition (Ba₄Ru₃O₁₀) was assumed for the structural refinement and provided a satisfactory fit.

High-Pressure Measurements

Elevated pressures were obtained by compressing the same single crystal described above within a modified Merrill-Bassett diamond anvil cell (13). A 4:1 mixture of methanol:ethanol was used as a hydrostatic pressure medium. Pressure was calibrated using fluorescence from ruby chips enclosed within the cell. Lattice parameter measurements for the sample at a pressure within the diamond anvil cell were obtained on a Picker four-circle diffractometer. The 8-reflection positions (13) of 11–15 reflections with $12.1° < 2\theta < 25.4°$ were fitted to determine a, b, and c. The reported values are those obtained via constrained fits in which the interaxial angles were presumed to be 90°. Unconstrained fits gave values within 1σ (the estimated standard deviation) of 90° for each of the angles in most cases, with all but one within 2σ. Full structural determinations were not repeated at high pressures.

RESULTS AND DISCUSSION

Crystal Structure

Refinement of the single-crystal data indicates an orthorhombic unit cell with the *Cmca* space group (No. 64) and lattice parameters of $a = 5.7762(15)$ Å, $b = 13.271(4)$ Å, and $c = 13.083(3)$ Å. The atomic coordinates and isotropic thermal parameters are listed in Table 2. Anisotropic thermal parameters are provided in Table 3.

TABLE 2
Atomic Coordinates and Isotropic Thermal Parameters for Ba₄Ru₃O₁₀

Atom	Site	x	y	z	β (Å²)
Ba(1)	8f	0	0.23978(4)	0.11127(4)	0.90(2)
Ba(2)	8f	0	0.53548(4)	0.13890(3)	0.73(2)
Ru(1)	4a	0	0	0	0.54(2)
Ru(2)	8f	0	0.87525(5)	0.14957(5)	0.51(2)
O(1)	8e	¼	0.3774(4)	¼	1.08(10)
O(2)	8f	0	0.0350(5)	0.1517(5)	0.79(9)
O(3)	16g	0.2708(7)	0.3906(3)	0.0346(3)	0.78(6)
O(4)	8f	0	0.7306(5)	0.1462(5)	1.36(11)

TABLE 3
Anisotropic Thermal Parameters[a] for Ba$_4$Ru$_3$O$_{10}$

Atom	U_{11}	U_{22}	U_{33}	U_{12}	U_{13}	U_{23}
Ba(1)	0.0106(3)	0.0069(3)	0.0167(3)	0	0	−0.0001(2)
Ba(2)	0.0098(3)	0.0078(3)	0.0101(3)	0	0	−0.0006(2)
Ru(1)	0.0076(4)	0.0058(4)	0.0072(4)	0	0	0.0004(3)
Ru(2)	0.0066(3)	0.0059(3)	0.0070(3)	0	0	−0.0002(2)
O(1)	0.013(3)	0.016(3)	0.012(3)	0	0.005(2)	0
O(2)	0.013(3)	0.006(3)	0.011(2)	0	0	−0.000(2)
O(3)	0.009(2)	0.009(2)	0.011(2)	−0.002(1)	−0.003(2)	0.003(1)
O(4)	0.020(3)	0.006(3)	0.026(4)	0	0	−0.002(2)

[a] Temperature factor $= \exp(-\sum_i \sum_j 2\pi^2 h_i h_j a_i^* a_j^* U_{ij})$, where h_i is a Miller index and a_i^* is the length of the ith reciprocal axis vector.

The structure reported here is of higher symmetry than the monoclinic ($P2_1/a$) structure reported earlier (8) on the basis of Rietveld refinement of X-ray powder diffraction data. The reported monoclinic unit cell ($a = 5.776$ Å, $b = 13.076$ Å, $c = 7.234$ Å, $\beta = 113.53°$) is nearly identical to the primitive cell of the $Cmca$ structure that we observed ($a = 5.7762(15)$ Å, $b = 13.083(3)$ Å, $c = 7.2373(19)$ Å, $\beta = 113.528(4)°$).[2] Calculated X-ray powder diffraction patterns based on the two structures are difficult to distinguish from one another, as shown in Fig. 1. The intensities of the reflections, the interaxial angles calculated from unconstrained refinements at both ambient and high pressures, comparison to similar compounds, and the quality of the final refinements all favor the orthorhombic assignment. The Inorganic Crystal Structure Database (ICSD) listing (14) based on the earlier monoclinic structural solution notes that whereas the temperature factors are self-consistent within the report, they are not all plausible or meaningful. Problems with refined thermal parameters are common when a structure is incorrectly refined in such a subgroup.

The monoclinic form described in the earlier work on Ba$_4$Ru$_3$O$_{10}$ (8) is isostructural with that determined for Ba$_4$Ir$_3$O$_{10}$ (15). Other reports on similar compounds indicated an orthorhombic $Cmca$ or $Cmc2_1$ unit cell for Ba$_4$(Ru, Mn)$_3$O$_{10}$ (16), Ba$_4$(Ti, Pt)$_3$O$_{10}$ (17), Ba$_4$(Ti, Ir)$_3$O$_{10}$ (18), and Ba$_4$Ir$_2$AlO$_{10}$ (19) and the ternary

[2] Values listed are for a monoclinic refinement of our current data; they are within measurement error of values obtained from transformation of the derived orthorhombic parameters. The transformation matrix for conversion of the C-centered orthorhombic unit cell axes to the primitive monoclinic unit cell axes is

$$\begin{bmatrix} 1 & 0 & 0 \\ 0 & 0 & -1 \\ -\frac{1}{2} & \frac{1}{2} & 0 \end{bmatrix}.$$

fluorides Cs$_4$$M$$_3F_{10}$ (M = Mg, Co, Ni, Zn) (20). Thus, although the $Cmca$ symmetry had not previously been observed for a ternary compound of $A_4B_3O_{10}$ stoichiometry, its presence in the case of Ba$_4$Ru$_3$O$_{10}$ is consistent with observations from the closely-related quaternary oxide and ternary fluoride compounds.

The structural building blocks closely resemble those reported in the earlier work. As shown in Fig. 2, the structure contains short chains of three face-sharing RuO$_6$ octahedra that are connected to other such groups at their terminal corners. Atoms of Ba are 10-fold and 11-fold coordinated by oxygen. There are, however, some minor differences. For example, the four O(3) atoms connecting the central RuO$_6$ octahedron in each group to the adjacent octahedra are equidistant from the central Ru(1) cation. The longest Ba–O bond distance of 3.661 Å reported in the earlier work appears to be an error; for the monoclinic unit cell proposed there (8), that specific distance is actually 2.661 Å and thus the longest Ba–O bond is 3.333 Å. The Ba–O bond distances in our revised structure are rather different and are listed in Table 4; they range from 2.592 to 3.391 Å.

Kafalas and Longo (7) were able to synthesize the end member ($n = 1$) of the barium ruthenate Ruddlesden–Popper series (9–11), layered Ba$_2$RuO$_4$, under conditions of $P = 6.5$ GPa and $T = 1200°$C. They had previously suggested that the other ($n = \infty$) end member, BaRuO$_3$ in the perovskite form, would be expected to stabilize at approximately 12 GPa (7, 21). This would indicate that a phase transition for Ba$_4$Ru$_3$O$_{10}$ might be expected between 6.5 and 12 GPa. In work by others, however, the synthesis of
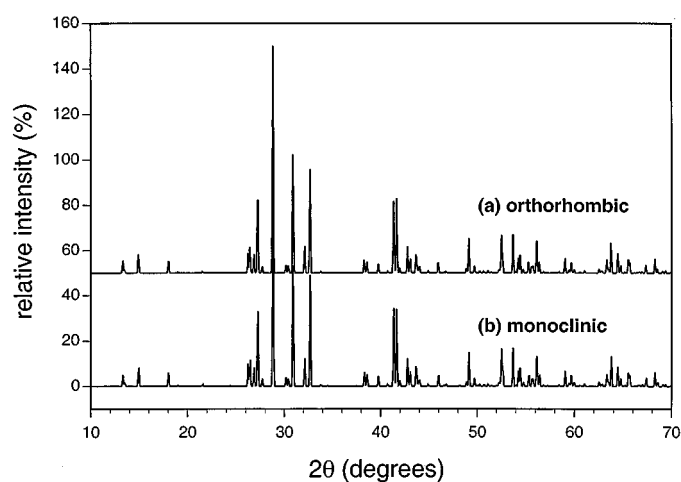

FIG. 1. Calculated powder X-ray diffraction patterns for (a) the orthorhombic $Cmca$ structure for Ba$_4$Ru$_3$O$_{10}$ derived in the present work and (b) the monoclinic ($P2_1/a$) structure reported earlier (8) (Cu$K\alpha$ source radiation).
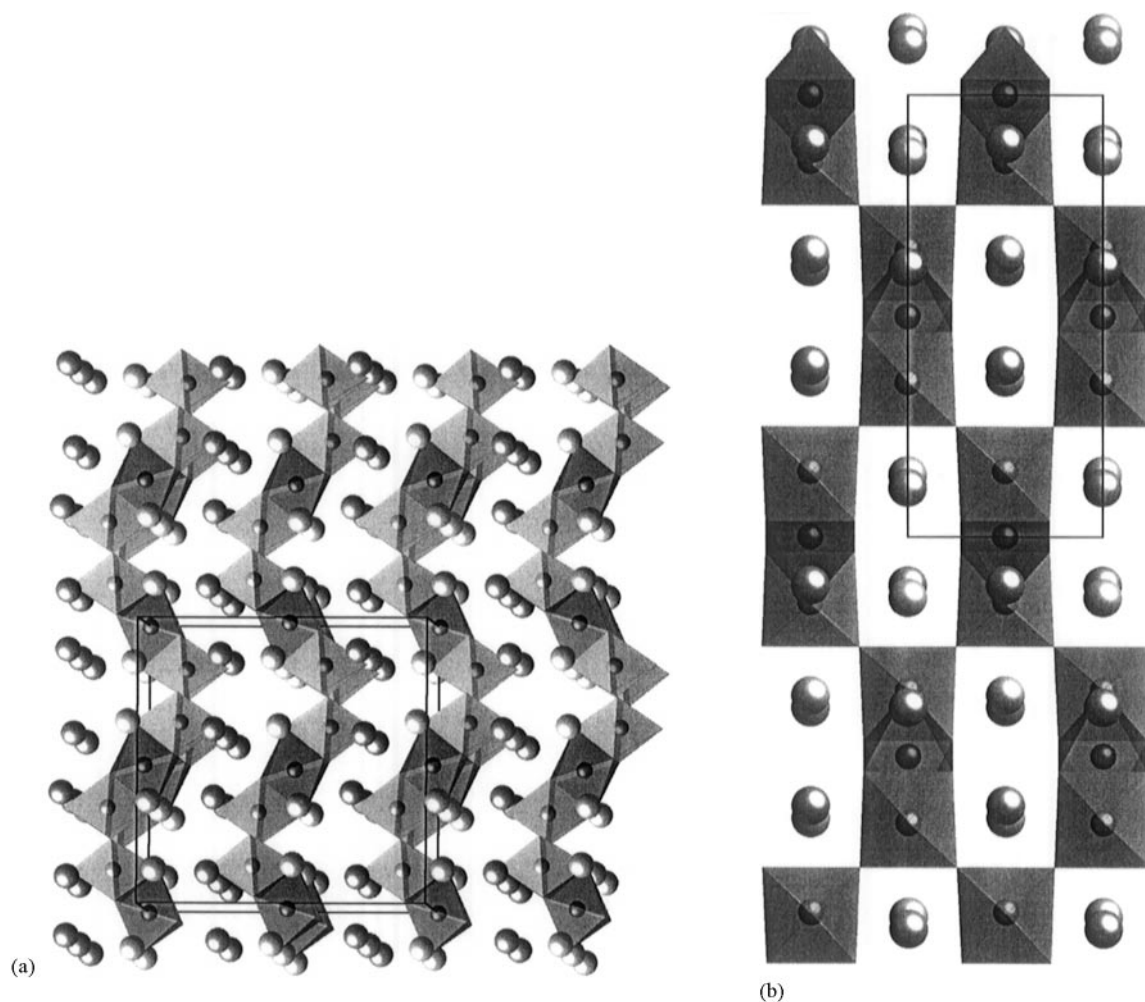
FIG. 2. (a) Projected view of the crystal structure of $Ba_4Ru_3O_{10}$ aligned nearly along [100] and (b) the crystal structure viewed along [010]. The Ru coordination polyhedra are drawn in as semitransparent blocks with the oxygen positions at the vertices. Cations are represented as small spheres (Ru) within and larger spheres (Ba) outside the octahedra. Several unit cells are shown to clarify the interrelationships of the structural units. In (b), only the nearest sets of RuO_6 octahedra are shown; in projection, the subsequent three-unit face-sharing chains along the viewing direction fall in the positions between those seen here.

layered Ba_2RuO_4 having lattice parameters consistent with the layered perovskite structure was reported without any apparent applied pressure during the synthesis (3, 6), suggesting that stabilization of Ruddlesden–Popper structures in barium ruthenates might not require as high a pressure as reported by Kafalas and Longo. In any event, no phase transition was observed in $Ba_4Ru_3O_{10}$ in our work at pressures up to 5.4 GPa. One might expect, however, that even if this transition were to be favored, the bond-breaking necessary to transform from the low-pressure to the high-pressure form would destroy a single crystal and thus maintenance (or recovery) of long-range order might not be feasible without a simultaneous increase of the temperature.

Anisotropic Compressibility

Figure 3 shows the variation of the lattice parameters as a function of pressure. The c axis is the direction of greatest compressibility, as is reasonable upon examination of the structure. In this direction, one can imagine that the zig–zag chains of RuO_6 octahedra can be readily folded in an accordion fashion at the corner-sharing linkages without substantial distortion of the individual coordination polyhedra. This type of behavior is similar to the polyhedral tilting that constitutes a type of displacive phase transition in other materials (22). In contrast, the lowest compressibility is along the b axis, which requires forcing the sheets of RuO_6 octahedra and the intervening layers of Ba atoms

TABLE 4
Selected Interatomic Distances and Bond Angles for Ba$_4$Ru$_3$O$_{10}$

	Distance (Å)		Angle (°)
Ru(1)–O(2) (× 2)	2.038(6)	O(3)–Ru(1)–O(3)	82.1(2)
Ru(1)–O(3) (× 4)	2.017(4)	O(3)–Ru(1)–O(3)	97.9(2)
Ru(2)–O(1) (× 2)	1.953(1)	O(3)–Ru(1)–O(3)	180.00
Ru(2)–O(2)	2.120(6)	O(3)–Ru(1)–O(2)	86.9(2)
Ru(2)–O(3) (× 2)	2.014(4)	O(3)–Ru(1)–O(2)	93.1(2)
Ru(2)–O(4)	1.920(7)	O(2)–Ru(1)–O(2)	180.00
Ru(1)–Ru(2) (× 2)	2.563(1)	O(1)–Ru(2)–O(1)	95.4(1)
Ba(1)–O(1) (× 2)	2.952(4)	O(1)–Ru(2)–O(2)	88.6(2)
Ba(1)–O(2)	2.769(6)	O(1)–Ru(2)–O(3)	90.8(1)
Ba(1)–O(3) (× 2)	2.731(4)	O(1)–Ru(2)–O(3)	170.8(2)
Ba(1)–O(3) (× 2)	2.896(4)	O(3)–Ru(2)–O(3)	82.2(2)
Ba(1)–O(4) (× 2)	2.927(1)	O(2)–Ru(2)–O(3)	84.8(2)
Ba(1)–O(4)	3.175(6)	O(4)–Ru(2)–O(1)	91.7(2)
Ba(1)–O(4)	3.391(6)	O(4)–Ru(2)–O(3)	94.8(2)
Ba(2)–O(1) (× 2)	2.932(4)	O(4)–Ru(2)–O(2)	180.00
Ba(2)–O(2) (× 2)	2.893(1)	Ru(2)–Ru(1)–Ru(2)	180.00
Ba(2)–O(3) (× 2)	2.829(4)		
Ba(2)–O(3) (× 2)	2.926(4)		
Ba(2)–O(4)	2.592(7)		
Ba(2)–O(2)	2.740(6)		

TABLE 5
Compressibility Data (Measured Lattice Parameters as a Function of Pressure)

Pressure (GPa)	a (Å)	b (Å)	c (Å)	V (Å^3)
0	5.7762(15)	13.271(4)	13.083(3)	1002.9(8)
0.18(3)	5.7738(9)	13.263(1)	13.073(2)	1001.2(2)
2.08(5)	5.7413(12)	13.208(2)	12.987(5)	984.8(5)
2.72(2)	5.7303(18)	13.187(2)	12.961(4)	979.4(4)
3.79(3)	5.7134(15)	13.156(2)	12.930(5)	971.9(4)
4.77(2)	5.6985(13)	13.132(1)	12.887(3)	964.4(3)
5.37(3)	5.6902(26)	13.114(3)	12.848(7)	958.8(6)

for a, b, and c in Å, P in GPa, and where R is the correlation coefficient for the fit. The corresponding linear compressibilities are $\beta_a = 0.0031$, $\beta_b = 0.0024$, and $\beta_c = 0.0034$ in units of GPa^{-1}. A listing of the measured lattice parameters at each pressure is included as Table 5.

Equation of State and Bulk Modulus

A plot of the unit cell volume as a function of pressure is included as Fig. 4. Fitting of this data to a Vinet equation of state (23, 24) with a fixed zero-pressure unit cell volume of $V_0 = 1002.91$ Å^3 (the measured value at ambient P) indicates a bulk modulus of $K_0 = 112.1(35)$ GPa with a derivative of $K'_0 = 3.8(17)$. Use of a Birch–Murnaghan expression (13) with fixed V_0 yields the same values ($K_0 = 112.1(35)$ GPa, $K'_0 = 3.8(16)$), as expected for a material that is not highly compressible. Weighted Vinet and Birch–Mur-

closer together. The lattice parameters decrease nonlinearly with positive curvature, as expressed below:

$$a = 5.7769(2) - 0.0179(3)P + 0.00032(7)P^2 \quad R = 0.9999,$$

$$b = 13.2693(8) - 0.0313(9)P + 0.00049(18)P^2 \quad R = 0.9997,$$

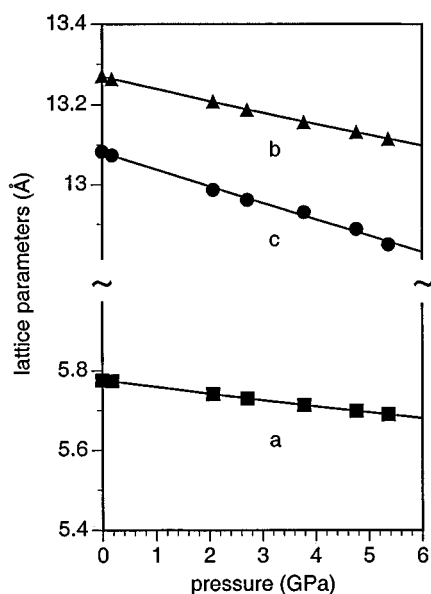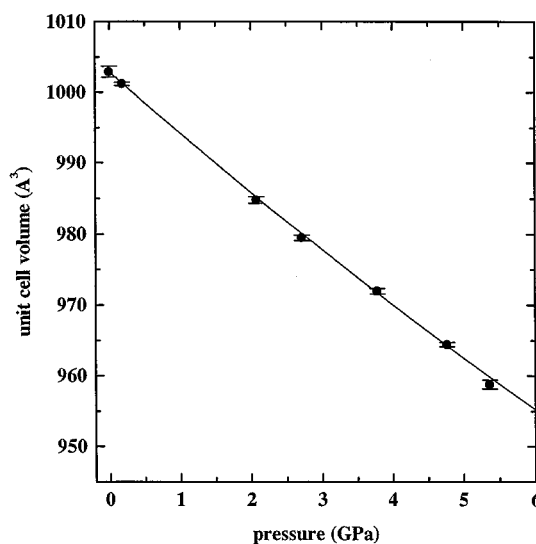$$c = 13.082(3) - 0.045(5)P + 0.0008(9)P^2 \quad R = 0.9973,$$

FIG. 3. Variation of the unit cell parameters (a, b, and c) as a function of pressure (P). The polynomial fits referenced in the text are shown for each data set.

FIG. 4. Variation of the unit cell volume (V) as a function of pressure (P). The estimated standard deviations in volume are as indicated by the bars, and the data have been fit to a Vinet equation of state as discussed in the text.

naghan fits in which V_0 is allowed to vary also provide nearly identical results (Vinet: $V_0 = 1002.911(1)$ Å^3, $K_0 = 113.3(47)$ GPa, and $K_0' = 3.4(20)$; Birch–Murnaghan: $V_0 = 1002.911(3)$ Å^3, $K_0 = 113.6(47)$ GPa, and $K_0' = 3.4(18)$). The standard deviation for K_0' is large but not surprising considering the limited pressure range examined.

ACKNOWLEDGMENTS

REFERENCES

1. J. J. Randall and R. Ward, *J. Am. Chem. Soc.* **81,** 2629 (1959).
2. P. C. Donohue, L. Katz, and R. Ward, *Inorg. Chem.* **4,** 306 (1965).
3. M. I. Gadzhiev and I. S. Shaplygin, *Russ. J. Inorg. Chem.* **29,** 1230 (1984).
4. T. L. Popova, N. G. Kisel, V. I. Krivobok, and V. P. Karlov, *Sov. Prog. Chem.* **48,** 8 (1982).
5. C. C. Torardi, *Mater. Res. Bull.* **20,** 705 (1985).
6. I. I. Prosychev and I. S. Shaplygin, *Russ. J. Inorg. Chem.* **25,** 489 (1980).
7. J. A. Kafalas and J. M. Longo, *J. Solid State Chem.* **4,** 55 (1972).
8. C. Dussarrat, F. Grasset, R. Bontchev, and J. Darriet, *J. Alloys Compd.* **233,** 15 (1996).
9. S. N. Ruddlesden and P. Popper, *Acta Crystallogr.* **10,** 538 (1957).
10. S. N. Ruddlesden and P. Popper, *Acta Crystallogr.* **11,** 54 (1958).
11. J. M. Longo and P. M. Raccah, *J. Solid State Chem.* **6,** 526 (1973).
12. C. Mallika and O. M. Sreedharan, *J. Alloys Compd.* **191,** 219 (1993).
13. R. M. Hazen and L. W. Finger, "Comparative Crystal Chemistry." Wiley, New York, 1982.
14. Inorganic Crystal Structure Database. Release 98/2. CD-ROM. Fachinformationszentrum Karlsruhe and Gmelin-Institut, Karlsruhe, 1999.
15. J. Wilkens and Hk. Müller-Buschbaum, *Z. Anorg. Allg. Chem.* **592,** 79 (1991).
16. M. Neubacher and Hk. Müller-Buschbaum, *Monatsh. Chem.* **121,** 635 (1990).
17. R. Fischer and E. Tillmans, *Z. Kristallogr.* **157,** 69 (1981).
18. Hk. Müller-Buschbaum and M. Neubacher, *Z. Anorg. Allg. Chem.* **586,** 87 (1990).
19. M. Neubacher and Hk. Müller-Buschbaum, *Z. Anorg. Allg. Chem.* **594,** 133 (1991).
20. R. E. Schmidt, J. Pebler, and D. Babel, *Eur. J. Solid State Inorg. Chem.* **29,** 679 (1992).
21. J. M. Longo and J. A. Kafalas, *Mater. Res. Bull.* **3,** 687 (1968).
22. R. M. Hazen and L. W. Finger, *Phase Transitions* **1,** 1 (1979).
23. P. Vinet, J. Ferrante, J. H. Rose, and J. R. Smith, *J. Geophys. Res.* **92,** 9319 (1987).
24. P. Vinet, J. Ferrante, J. R. Smith, and J. H. Rose, *J. Phys. C* **19,** L467 (1986).